

A Practical Wavelength Division Demultiplexer for Short Wavelength Local Area Networks

Jian Liu and Ray T. Chen

Microelectronics Research Center
Department of Electrical and Computer Engineering
University of Texas at Austin
Austin, Texas 78758

ABSTRACT

Using a beveled-edge to couple optical signals into a waveguiding plate, a path-reversed substrate-guided wave holographic interconnection is employed for a WDDM with a channel wavelength spacing as small as 2 nm. A waveguide grating with a 45° incident angle and a 45° diffraction angle is fabricated using 20 μm thick DuPont photopolymer film HRF 600x001. The dispersion and the 3 dB bandwidth of the device are measured to be $0.18^\circ/\text{nm}$ and 20 nm, respectively. A four-channel wavelength demultiplexing is demonstrated at 796 nm, 798 nm, 800 nm, and 802 nm with no crosstalk observed. A one-to-five cascaded 4-channel WDDM with $\pm 5\%$ energy uniformity under an s-polarization is also demonstrated to increase the user-sharing capacity. Twenty fanout channels (5x4) are experimentally achieved.

Keywords: wavelength division multiplexing; volume holographic grating; photopolymer films; optical interconnects; dispersion.

1. Introduction

In optical communications, wavelength division multiplexing (WDM) is employed as a powerful approach to significantly increase the capacity of the fiber transmission lines. At the end of a transmission line, a WDDM is always employed to separate optical channels of different wavelengths and to route optical signals to their designated users. For long haul telecommunications at wavelengths of 1330 nm and 1550 nm, investigators have been primarily focusing on two kinds of grating-based approaches. They are arrayed waveguide gratings (AWG)¹⁻⁶, and fiber Bragg gratings⁷⁻¹¹. The dispersion of the AWG is caused by the length differences of the arrayed waveguides. The wavelength selectivity of a fiber Bragg grating is due to a relatively long fiber grating with a small refractive index modulation. In data communications, where interconnection distance is relatively short, usually within 1 km, it is intended to use short wavelengths, for example 800 nm, in conjunction with a multimode fiber to transmit optical signals. In this scenario, optical transceivers are mature and the aggregate bandwidth can meet the system requirements¹²⁻¹⁶.

For previous substrate-guided-wave holograms^{17, 18}, optical signals of various wavelengths are dispersed by an input holographic grating, propagating within a waveguiding plate with total internal reflection (TIR), and then coupled out of the substrate by output holographic gratings. The interchannel wavelength separation of such a WDDM is totally dependent on the length between the input and the output couplers. To obtain a smaller channel wavelength spacing, employment of a long substrate is a necessity. Meanwhile, a lens array is always needed to couple the output optical signals with different wavelengths into a fiber array. In our proposed path-reversed substrate-guided-wave optical interconnects, instead of using an input holographic grating, a beveled edge is used to couple optical signals into the waveguiding plate with an angle larger than the critical angle of the plate, and a DuPont photopolymer-based holographic grating is employed to separate the optical signals of different wavelengths. It is a path-reversed structure because the optical signals are dispersed by the output waveguide hologram. The input light comes from the waveguiding plate and the diffracted light goes into the air. Only one lens is used to couple the dispersed optical signals into their designated fibers. Moreover, multiple fanouts can be realized by integrating a cascaded holographic grating array on the same waveguiding plate.

2. Working principles

2.1 Photopolymer films

DuPont (DuPont Holographic Materials, Wilmington, Delaware, USA) provides promising holographic film due to its dry processing, long shelf life, good photo-speed, and large index modulation²⁰⁻²³. The holographic photopolymer is usually coated from solvent onto a clear support, typically Mylar polyester film. A removable cover sheet is used as a protecting cover. The thicknesses of photopolymer are available from 10 to 100 μm . The hologram formation mechanism in the photopolymer films is known to be a three-step process. First, an exposure initiates the interference pattern, which causes initial polymerization and diffusion of the monomer molecules to bright fringe areas from the dark fringe neighborhoods in the photopolymer. A higher concentration of polymerization means a higher refractive index. Second, a uniform UV light is required for dye bleaching and complete polymerization. Third, a baking process can further enhance the refractive index modulation of the hologram formed in the photopolymer film. It is shown that the dynamic properties of diffraction efficiency versus exposure time can be controlled by the two recording beam intensities, which are related with the polymerization rates and the diffusion rates in the photopolymer films²¹.

2.2 Dispersion and bandwidth of the path-reversed substrate-guided-wave holograms

Fig. 1(a) shows the structure of the proposed path-reversed substrate-guided-wave interconnect scheme. Collimated optical signals with different wavelengths are coupled into a waveguiding plate with an Aluminum-coated beveled edge of an angle α , zig-zagging within the substrate with a bouncing angle larger than the critical angle of the waveguiding plate, and then coupled out by the photopolymer-based volume holographic grating fabricated on one side of the substrate. The dispersed optical signals can be coupled by a focusing-lens into a fiber array. The thickness of the waveguiding plate is t . Fig. 1(b) shows the detailed structure of the volume holographic grating with a thickness of d . The grating has a period of Λ and a slanted angle of ϕ . The grating equation is given by¹⁹

$$\Lambda_y (\sin\theta_2' + \sin\theta_2) = m \lambda / n, \quad m = 0, \pm 1, \pm 2, \dots \quad (1)$$

where θ_2 and θ_2' are the incident and the diffraction angles of the optical signals in the holographic grating region at the center wavelength of λ (in the air), respectively. n is the average refractive index of the holographic grating region. $\Lambda_y = \Lambda / \sin \phi$ is the grating period projected in Y direction. m represents the m th order for forward diffraction. In our case, m is equal to 1. Let θ_{diff} be the designed diffraction angle in the air of refractive index n_3 and θ the bouncing angle, i.e., the incident angle at the interface between the waveguiding plate and the grating. From the shown geometry of the beveled edge, we have $\theta = 2\alpha$.

The dispersion of the grating can be derived by differentiating Eq. (3.1), which gives

$$\begin{aligned} d\theta_{\text{diff}} / d\lambda &= \sin\phi / \Lambda \cos\theta_{\text{diff}} \\ &= n (\sin\theta_2' + \sin\theta_2) / \lambda \cos\theta_{\text{diff}}, \end{aligned} \quad (2)$$

From the geometry of Fig. 3.1 (c), the slanted angle ϕ of the grating and the grating period Λ are given by

$$\phi = \pi / 2 + (\theta_2' - \theta_2) / 2; \quad (3)$$

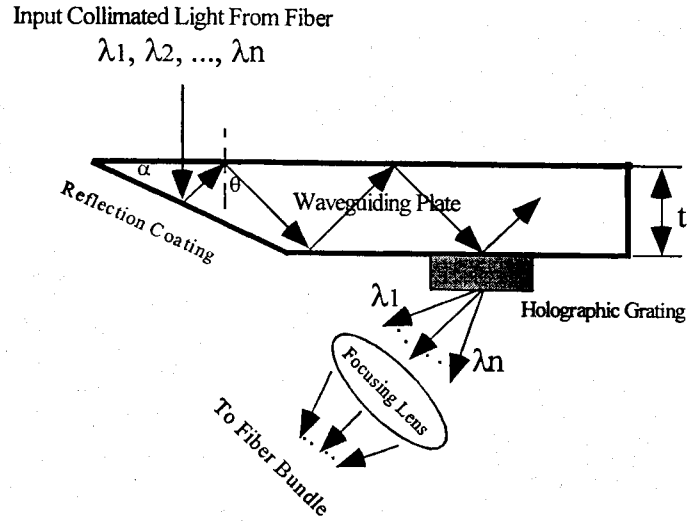
and

$$\Lambda = \lambda / 2 n \sin [(\theta_2' + \theta_2) / 2]. \quad (4)$$

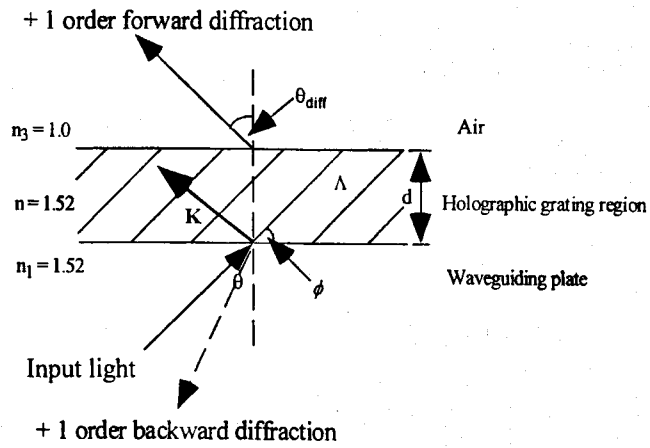
respectively, in which θ_2' and θ_2 are calculated from the designed values of θ_{diff} and θ using the Snell's Law.

Fig. 2(a) plots grating dispersion as a function of diffraction angle at incident angles of 0° , 30° , 45° , 60° , and 75° by using Eq. (2) at center wavelength of 800 nm. Incident angles of 0° and 30° are plotted in Fig. 2 for comparison. The

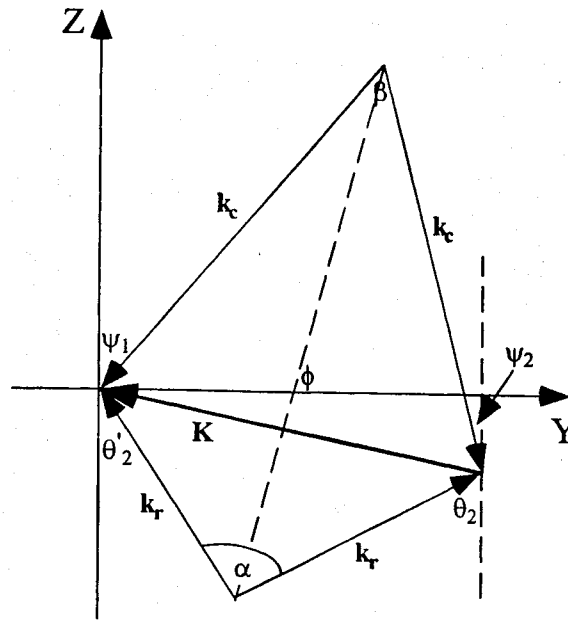
thickness of the guided-wave holographic gratings is 20 μm . The refractive indices are $n_1 = 1.0$, $n = n_3 = 1.52$. It is clearly indicated that higher dispersion occurs for a grating with a larger incident angle and a larger diffraction angle.



(a)



(b)



(c)

Figure 1 A path-reversed substrate-guided wave optical interconnection. (a) structure; (b) guided-wave holographic grating; (c) phase-matching condition for recording and reconstruction of the grating.

In design of a WDDM using a dispersion grating, the spectral bandwidth $\Delta\lambda$ of the grating has to accommodate all wavelength channels demultiplexed. The approximate spectral bandwidth is given by Ludman²⁴ in the form of

$$\Delta\lambda / \lambda = \Lambda \cos \theta_2' \sin \phi / d \sin \theta_2' \quad (5)$$

which is plotted in Fig. 2 (b). Table 1 shows the calculated parameters for four guided-wave grating structures. There exists a trade-off between the dispersion and the bandwidth of the guided-wave holographic gratings.

2.3 Hologram recording parameters

Fig. 1(c) shows the phase matching diagram for all the wavevectors in the holographic medium. The recording wave vector k_c ($|k_c| = 2\pi n' / \lambda_c$) are phase-matched with the grating vector K ($|K| = 2\pi / \Lambda$), and so does the reconstruction wave vector k_r ($|k_r| = 2\pi n / \lambda$) and K . n' is the average refractive index of the guided-wave holographic emulsion at recording wavelength λ_c . From the geometry of Fig. 1(c), the recording angles in the hologram medium of the two recording beams at wavelength λ_c are derived and given by

$$\psi_1 = \pi / 2 - (\phi - \beta / 2), \quad (6)$$

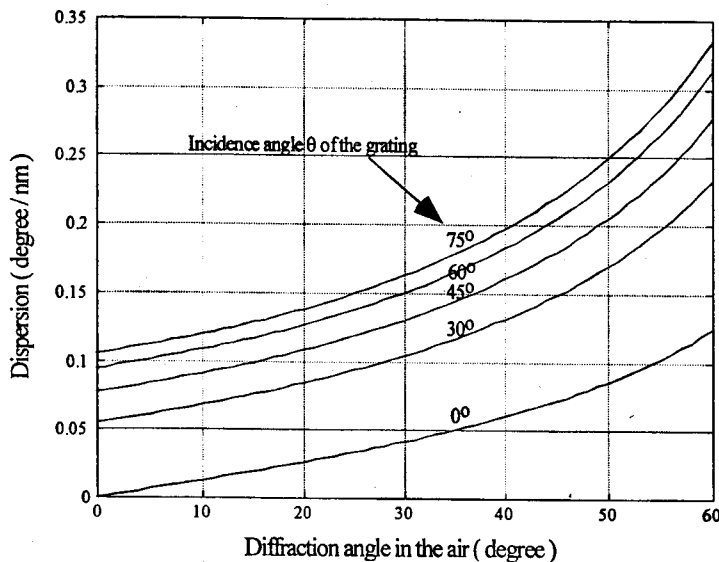
and

$$\psi_2 = (\phi + \beta / 2) - \pi / 2. \quad (7)$$

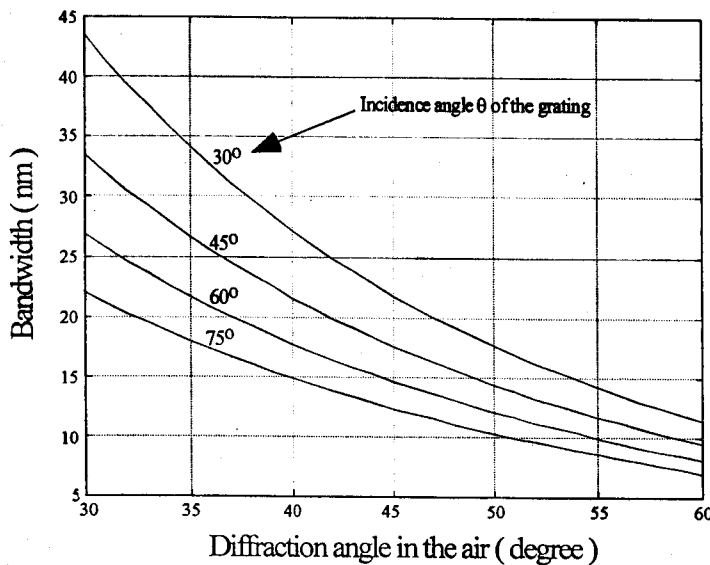
where

$$\beta = 2 \sin^{-1} \{ (n \lambda_c / n' \lambda) \sin[(\theta_2' + \theta_2) / 2] \}, \quad (8)$$

which is the angle between two recording beams. Note that the phase matching condition in Fig. 1(c) is in the holographic medium. In practice, the recording angles calculated by Eqs. (6) and (7) must be converted into those angles in the air by the Snell's Law.



(a)



(b)

Figure 2 (a) Dispersion calculated by Eq. (2); (b) bandwidth calculated by Eq. (5).

It is obvious that the absolute values of the two recording angles in the air can not be over 90° . Otherwise, a prism or other higher index medium must be used in the recording process. To justify the proposed approach, numerous cases are simulated and four cases are summarized in Table 3.1. Among the four cases shown in Table 1, case 2 has a reasonably high dispersion, and an acceptable bandwidth. Moreover, this kind of structure is easy to be fabricated. Note that the working principle presented herein is not only suitable for 800 nm but also for 1300 and 1550 nm.

Table 1 Parameters of four guided-wave holographic gratings

Case	α	θ	θ_{diff}	Λ	ϕ	$d\theta_{\text{diff}}/d\lambda$	B.W.
1	22.5	45	30	495.2	77.1	0.13	33
2	22.5	45	45	444.6	81.4	0.18	18
3	22.5	45	60	411.2	84.9	0.28	9.4
4	30	60	60	358.3	77.4	0.31	8.1

Note: all angles are in degree and grating period and wavelength are in nm. B.W. stands for bandwidth.

3. Experiment

3.1 WDDM working in the 800 nm region

We use a 514 nm Argon ion laser to record the output holographic grating. The reconstruction wavelength is designed to be at 800 nm. A Ti: Sapphire tunable laser is employed to characterize the performance of the device. DuPont photopolymer film HRF 600x001-20 with a thickness of 20 μm is chosen to record the guided-wave holographic grating. The waveguiding plate has a thickness of 6.3 mm. The beveled angle α is 22.5° , and the diffraction angle θ_{diff} in the air is 45° .

In our experiment, +1 order backward diffraction is observed to be about 15% of the intensity of the +1 order forward diffraction, which can be interpreted by the rigorous coupled wave analysis (RCWA)²⁵, as conceptually depicted in Fig. 3. The decomposed space-harmonic components of total field in the grating region allowed to be coupled into the glass plate region (backward diffraction) and the air (forward diffraction) include a +1 order forward diffraction and a +1 order backward diffraction. Other diffraction orders are cutoff outside the grating region. It is shown from Fig. 3 that backward diffraction orders always exist as long as forward diffraction orders exist, because of larger refractive index in region 1 (waveguiding region). The existing +1 order backward diffraction takes a certain percentage of input energy. This part of energy might be used for on-site channel monitoring of the WDDM.

Fig. 4 shows the measured dispersion of the WDDM. Theoretical results calculated by Eq. (2) are also shown in the figure as solid line. It is obvious that the experimental results are consistent with the theoretical expectations. The dispersion is found to be insensitive to the states of input polarization. Fig. 5 gives the measured diffraction efficiencies of the +1 order forward diffraction as a function of wavelength under different states of polarization. The diffraction efficiency is defined as the intensity of the +1 order forward diffraction divided by the intensity of the optical signal entering the WDDM device (not the output waveguide grating). Actually, before the optical signal impinges on the grating, it experiences losses of Fresnel reflection at the air-glass and the reflection-coating interfaces, and absorption and scattering of the waveguiding glass plate. Therefore, the actual diffraction efficiencies of the grating are larger than those given in Fig. 5. The 3dB bandwidth of this device is determined to be 20 nm, which is close to that given in Table 3.1. The discrepancy of the diffraction efficiencies between p- and s- polarization states shows this device is polarization sensitive. Theoretical analysis by the rigorous coupled wave analysis will be given in later publications.

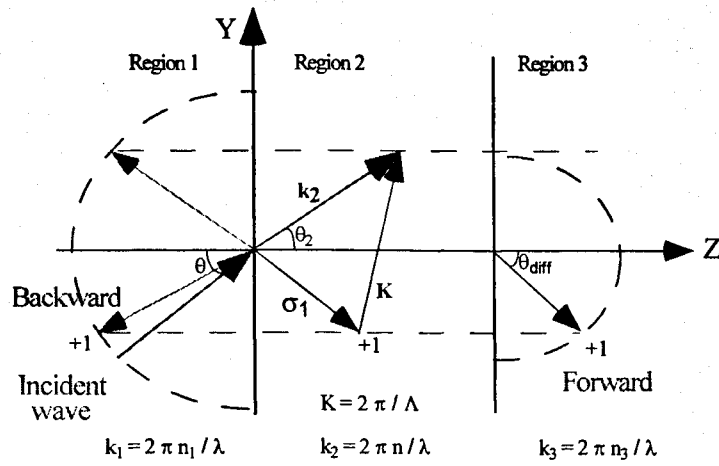


Figure 3 Conceptual interpretation of forward and backward diffractions by rigorous coupled wave analysis.

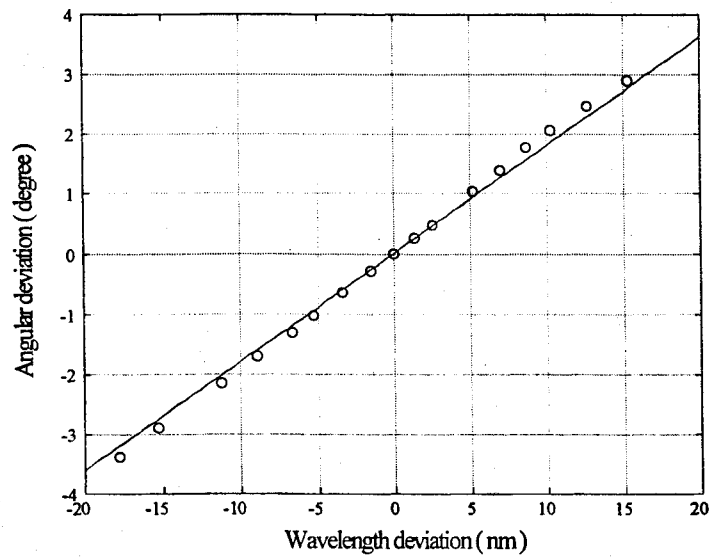


Figure 4 Experimental results (o) and theoretical expectations (solid line) of angular deviation as a function of wavelength change at center wavelength of 800 nm.

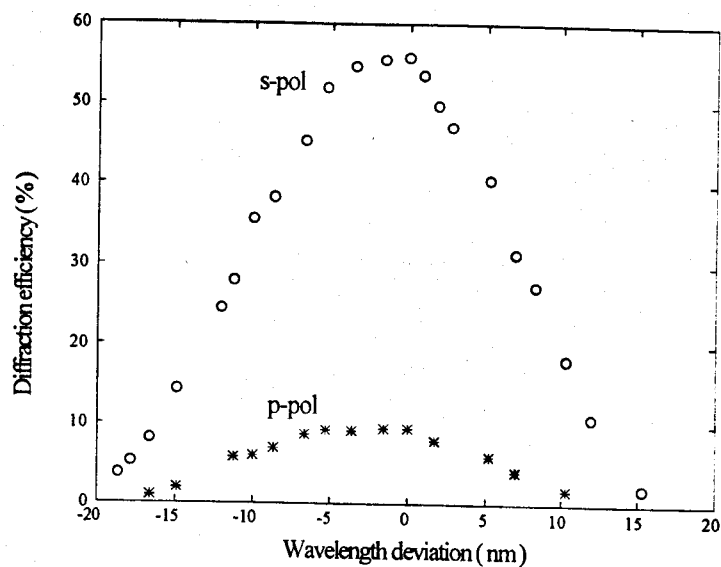


Figure 5 Measured diffraction efficiency as a function of wavelength deviation at the center wavelength of 800 nm under an s-wave and a p-wave.

Fig. 6 is an experimental result of a four-channel WDDM operating at 796 nm, 798 nm, 800 nm, and 802 nm, for which the bandwidth of the device can accommodate all the four-channel, as shown in Fig. 5, while maintaining a 2 nm wavelength separation. This image is taken by a CCD camera from the focal plane of a lens with a focal length of 20 cm. From Fig. 6, we can see that the four-channel are totally separated. There is no crosstalks observed in our experiment. Using an aspheric lens, it is possible to focus the light beams much smaller and to couple them into standard fiber bundles/arrays.

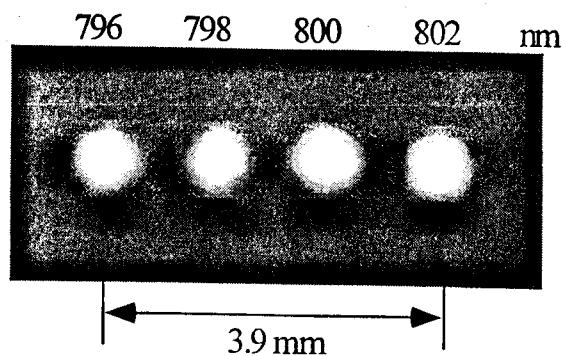


Figure 6 A CCD image of the light spots for this WDDM operating at 796 nm, 798 nm, 800 nm, and 802 nm.

3.2 A path-reversed substrate-guided-wave optical interconnect with multiple fanouts

To further increase the capacity and reduce the cost, we design a path-reversed substrate-guided-wave based WDDM with a multi-fanout feature. Fig. 7 shows that N cascaded volume holographic gratings are integrated on the same waveguiding plate, and the optical signals with different wavelengths are zig-zagged within the plate and coupled sequentially out of the substrate by the cascaded gratings. For each individual fanout, the dispersed wavelengths can be focused and coupled into optical fiber arrays. If each holographic grating is capable of separating M wavelengths, such a WDDM has a channel capacity of $N \times M$, N times larger than that described in last section. One important issue relating this device is to obtain a uniform fanout energy distribution, which can be found elsewhere²⁶⁻³⁰.

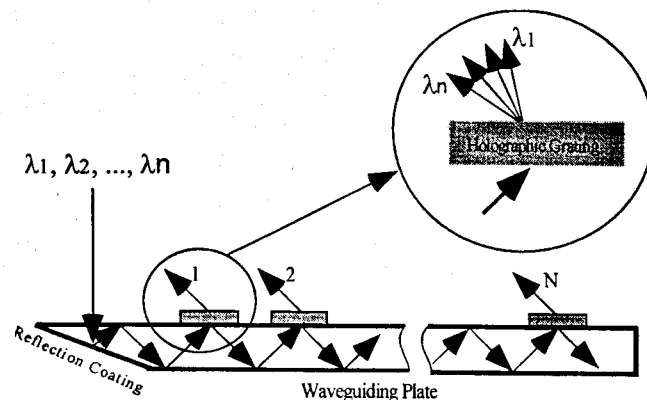


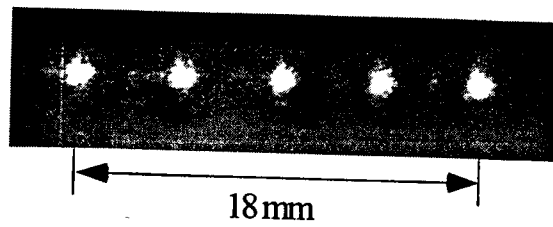
Figure 7 A path-reversed substrate-guided wave optical interconnection with multi-fanouts for WDDM application

Using the same grating parameters as mentioned before, and a beveled waveguiding plate with a thickness of 3.2 mm, five cascaded holograms are sequentially recorded on the same substrate by using DuPont photopolymer film HRF 600 with a thickness of 20 μm . Fig. 3.8 shows a CCD image of the device operating at center wavelength of 800 nm under an s-polarization. A three-dimensional intensity profile is also given in Fig. 8(b). Fanout energy distribution uniformity is measured to be within $\pm 5\%$. For each individual fanout, four-channels with a channel wavelength separation of 2 nm are also obtained as those shown in Fig. 6. With this large user sharing capability, the device is promising for data communications.

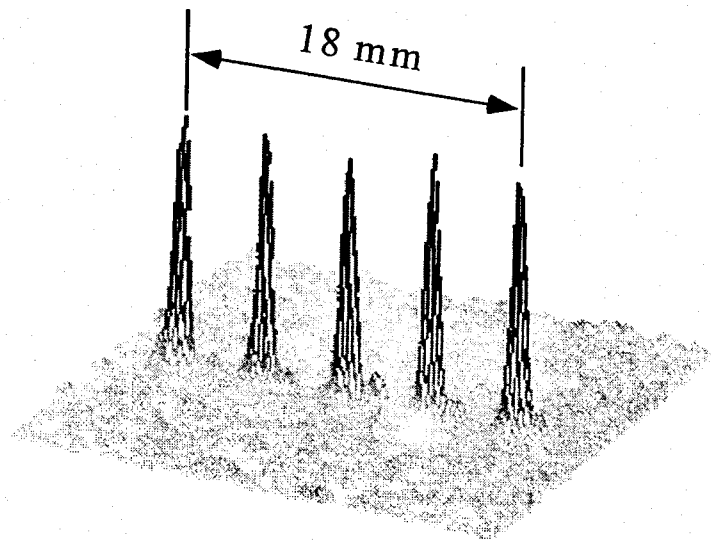
4. Discussion and conclusion

A low-cost packaging of a wavelength division demultiplexer (WDDM) is demonstrated at wavelengths of 750 nm, 780 nm, 810 nm, and 840 nm. This packaging is of potential to be used in short distance data communications. The insertion losses are 8.28 dB, 9.41 dB, 6.78 dB, and 11.71 dB, respectively.

A novel multi-wavelength photopolymer-based path-reversed substrate-guided-wave optical interconnect is presented to reduce the wavelength separation down to 2 nm. Both 800 nm and 1555 nm band can be realized using the proposed idea. The dispersion and the bandwidth of the guided-wave holograms are analyzed. It is shown that by adjusting the incident angle and the diffraction angle of the path-reversed structure the dispersion can be enhanced. Incident angle larger than the critical angle of the substrate can be obtained by beveling one edge of the waveguiding plate. The bulky waveguiding glass plate provides mechanical and environmental robustness. As the dispersion occurs for the output holographic grating, the TEM_{00} mode profile of the dispersed optical signals with different optical wavelengths is well-retained, and this also reduces the difficulties in integration with fiber array/bundles.



(a)



(b)

Figure 3.8 Experimental results of a one-to-five fanout WDDM operating at center wavelength of 800 nm. (a) CCD image; (b) 3-D intensity profile.

In our experiment, DuPont photopolymer film HRF 600x001-20 (20 μm thick) is chosen to record the holographic grating. The beveled angle of the waveguiding plate is $\alpha = 22.5^\circ$, and the diffraction angle of the holographic grating in the air is designed to be at 45° . The measured dispersion results are consistent with the theoretical analyses and are polarization-insensitive. A bandwidth of 20 nm is obtained for such a polarization-sensitive device (in terms of diffraction efficiency). A four-channel WDDM separating wavelengths of 796 nm, 798 nm, 800 nm, and 802 nm is demonstrated with

no channel crosstalk. Furthermore, this structure can incorporate with cascaded hologram arrays to obtain multiple fanouts for increasing the user-sharing capacity and reducing the cost of the device. A one-to-five fanout WDDM is fabricated with energy fluctuation within $\pm 5\%$ under an s-polarization at center wavelength of 800 nm. It is promising for this path-reversed substrate-guided-wave optical interconnect to be used as WDDM in data communications.

Acknowledgments: This research is supported by Ballistic Missile Defense Organization, Army SSDC, the Center of Optoelectronics Science and Technology (COST), DARPA, Office of Naval Research, AFOSR, Cray Research, DuPont, Lightpath, 3M Foundation, RRI, and the Advanced Technology Program (ATP) of the state of Texas.

References:

1. M. K. Smit, "New focusing and dispersive planar component based on an optical phased array," *Electron. Lett.* **24**, 385-386 (1988).
2. H. Takahashi, S. Suzuki, K. Kato, and I. Nishi, "Arrayed-waveguide grating for wavelength division multi/demultiplexer with nanometer resolution," *Electron. Lett.* **26**, 87-88 (1990).
3. C. Dragon, C. H. Henry, I. P. Kaminow, and R. C. Kistler, "Efficient multichannel integrated optics star coupler on silicon," *IEEE Photon. Technol. Lett.* **1**, 241-243 (1989).
4. C. Dragon, "An NxN optical multiplexer using a planar arrangement of two star couplers," *IEEE Photon. Technol. Lett.* **3**, 812-815 (1991).
5. C. Dragon, C. A. Edwards, and R. C. Kistler, "Integrated optics NxN multiplexer on Silicon," *IEEE Photon. Technol. Lett.* **3**, 896-899 (1991).
6. M. K. Smit and C. van Dam, "PHASAR-based WDM devices: principles, design and applications," *IEEE J. Selected Topics in Quantum Electron.* **2**, 236-250 (1996).
7. K. O. Hill, Y. Fujii, D. C. Johnson, and B. S. Kawasaki, "Photo-sensitivity in optical fiber waveguides: application to reflection filter fabrication," *Appl. Phys. Lett.* **32**, 647-649 (1978).
8. B. S. Kawasaki, K. O. Hill, D. C. Johnson, and Y. Fujii, "Narrow-band Bragg reflectors in optical fibers," *Opt. Lett.* **3**, 66-68 (1978).
9. F. Bilodeau, D. C. Johnson, S. Theriault, B. Malo, J. Albert, and K. O. Hill, "An all-fiber dense-wavelength-division multiplexer/demultiplexer using photoimprinted Bragg gratings," *IEEE Photon. Technol. Lett.* **7**, 388-390 (1995).
10. I. Baumann, J. Seifert, W. Nowak, and M. Sauer, "Compact all-fiber add-drop-multiplexer using fiber Bragg gratings," *IEEE Photon. Technol. Lett.* **8**, 1331-1333 (1996).
11. K. O. Hill and G. Meltz, "Fiber Bragg grating technology fundamentals and overview," *J. Lightwave Technol.* **15**, 1263-1276 (1997).
12. G. W. Neudeck, J. Denton, J. D. Schaub, R. Li, C. L. Schow, and J. C. Campbell, "A high speed Si photodiode by epitaxial lateral growth," *The 56th Annual Device Research Conference Digest*, Charlottesville, Virginia, June 22-24, 1998.
13. C. Schow, J. Schaub, R. Li, J. Qi, and J. C. Campbell, "A 1Gb/s monolithically integrated Silicon NMOS optical receiver," To be published in *IEEE Quantum Electronic Devices*, 1998.
14. S. Hu, J. Ko, and L. A. Coldren, "High-performance densely packed vertical-cavity photonic integrated emitter arrays for direct-coupled WDM applications," *IEEE Photon. Technol. Lett.* **10**, 766-768 (1998).

15. D. L. Huffaker and D. G. Deppe, "Multiwavelength, densely packed 2x2 vertical-cavity surface-emitting laser array fabricated using selective oxidation," *IEEE Photon. Technol. Lett.* **7**, 858-860 (1996).
16. S. Y. Hu, J. Ko, O. Sjolund, and L. A. Coldren, "Optical crosstalk in monolithically-integrated multiple wavelength vertical-cavity laser arrays for multimode WDM local area networks," *Electron. Lett.* **34**, 676-678 (1998).
17. M. M. Li and R. T. Chen, "Five-channel surface-normal wavelength-division demultiplexer using substrate-guided waves in conjunction with a polymer-based Littrow hologram," *Opt. Lett.* **20**, 797-799 (1995).
18. Y. K. Tsai, Y. T. Huang, and D. C. Su, "Multiband wavelength-division demultiplexing with a cascaded substrate-mode grating structure," *Appl. Opt.* **34**, 5582-5588 (1995).
19. R. R. A. Syms, *Practical Volume Holography*, Clarendon Press (Oxford, 1990).
20. W. Gambogi, K. Steijn, S. Mackara, T. Duzik, B. Hamzavy, and J. Kelly, "HOE imaging in DuPont holographic photopolymers," *Proc. SPIE* **2152**, 282-293 (1994).
21. U. Rhee, H. J. Caulfield, C. S. Vikram, and J. Shamir, "Dynamics of hologram recording in DuPont photopolymer," *Appl. Opt.* **34**, 846-853 (1995).
22. S. Piazzolla and B. K. Jenkins, "Holographic grating formation in photopolymers," *Opt. Lett.* **21**, 1075-1077 (1996).
23. H. J. Zhou, V. Morozov, and J. Neff, "Characterization of DuPont photopolymers in infrared light for free-space optical interconnects," *Appl. Opt.* **34**, 7457-7459 (1995).
24. J. E. Ludman, "Approximate bandwidth and diffraction efficiency in thick holograms," *Am. J. Phys.* **50**, 244-246 (1982).
25. T. K. Gaylord and M. G. Moharam, "Analysis and applications of optical diffraction by gratings," *Proc. IEEE* **73**, 894-937 (1985).
26. Jian Liu and Ray T. Chen, "Substrate-guided-wave-based optical interconnects for multi-wavelength routing and distribution networks," To be published in *J. Lightwave Technol.* 1999.
27. T. Nakaya, Y. Katoh, T. Kubota, and M. Tabeda, "Diffraction efficiency of a grating coupler for an array illuminator," *Appl. Opt.* **35**, 3891-3898 (1996).
28. Jian Liu, Chunhe Zhao, R. Lee, and Ray T. Chen, "Cross-link optimized cascaded volume hologram array with energy-equalized one-to-many surface-normal fan-outs," *Opt. Lett.* **22**, 1024-1026 (1997).
29. Jian Liu, Zhenhai Fu, Ray T. Chen, "Polarization sensitivity of photopolymer-based volume holograms for one-to-many surface normal optical interconnects," *Opt. Eng.* **37**, 660-665 (1998).
30. Jian Liu and Ray T. Chen, "A two-dimensional dual-wavelength routing network with 1-to-10 cascaded fanouts," *IEEE Photon. Technol. Lett.* **10**, 238-240 (1997).